stochastic theory thus gives some insight into the nature of these approximations. In our central result, Eq. (24), a relaxation superoperator $\mathcal{W}$ appears. This superoperator must, in a stochastic treatment, be treated as input information, to be specified as part of the physical circumstances of the problem. In an *ab initio* calculation this superoperator is in principle determined by the Hamiltonian, but in practice[8] the matrix elements are specified.

In a future paper we will discuss the application of our formalism to a number of specific cases in Mössbauer spectra. It is clear, however, that the theory is of utility in analyzing perturbed angular-correlation spectra and line shapes in other branches of spectroscopy as well.

*Work supported by the United States Atomic Energy Commission.

[1]M. Blume, Phys. Rev. Letters 14, 96 (1965).
[2]F. van der Woude and A. J. Dekker, Phys. Status Solidi 9, 775 (1965).
[3]H. Wegener, Z. Physik 186, 498 (1965).
[4]H. H. Wickman, M. P. Klein, and D. A. Shirley, Phys. Rev. 152, 345 (1966).
[5]M. Blume and J. A. Tjon, Phys. Rev. 165, 446 (1968); J. A. Tjon and M. Blume, *ibid.* 165, 456 (1968).
[6]A. M. Afanas'ev and Yu. Kagan, Zh. Eksperim. i Teor. Fiz 45, 1660 (1963) [Soviet Phys. JETP 18, 1139 (1964)].
[7]E. Bradford and W. Marshall, Proc. Phys. Soc. (London) 87, 731 (1966).
[8]H. Gabriel, J. Bosse, and K. Rander, Phys. Status Solidi 27, 301 (1968).
[9]L. L. Hirst, J. Phys. Chem. Solids 31, 655 (1970).
[10]H. Schwegler (unpublished).
[11]P. W. Anderson, J. Phys. Soc. Japan 9, 316 (1954).
[12]R. Kubo, in *Fluctuation, Relaxation and Resonance in Magnetic Systems*, edited by D. ter Haar (Oliver and Boyd, Edinburgh, Scotland, 1962), p. 23.
[13]A. Abragam, *The Principles of Nuclear Magnetism* (Oxford U. P., London, England, 1961).
[14]A. Abragam and R. V. Pound, Phys. Rev. 92, 943 (1953).
[15]R. M. Steffen and H. Frauenfelder, in *Perturbed Angular Correlations* (North-Holland, Amsterdam, 1964).
[16]M. Blume, in *Hyperfine Structure and Nuclear Radiations* (North-Holland, Amsterdam, 1968), p. 911.
[17]A preliminary report on this work was given earlier by M. J. Clauser and M. Blume, Bull. Am. Phys. Soc. 15, 260 (1970).
[18]M. Blume, Phys. Rev. 174, 351 (1968).
[19]M. C. Wang and G. Uhlenbeck, Rev. Mod. Phys. 17, 323 (1945).
[20]R. L. Stratonovich, *Topics in the Theory of Random Noise* (Gordon and Breach, New York, 1963), Vol. I, p. 143.
[21]R. Zwanzig, J. Chem. Phys. 33, 1338 (1960); Physica 30, 1109 (1964).
[22]In particular, compare Table I of Ref. 18 with our Table II. By specializing both examples to treat the same case, the similarities of both treatments may be seen.
[23]Cf. Eq. (16) of Ref. 11.
[24]M. J. Clauser and R. L. Mössbauer, Phys. Rev. 178, 559 (1969).
[25]We emphasize that $T_{\mu\nu}$ denotes an operator, *not* the matrix element $\langle\mu|T|\nu\rangle$.
[26]L. D. Landau and E. Lifshitz, *Statistical Physics* (Pergamon, New York, 1958), p. 20.

PHYSICAL REVIEW B VOLUME 3, NUMBER 3 1 FEBRUARY 1971

Mössbauer Effect of Sn^{119} in Alpha-Brass and Related Alloy Systems*†

Joseph K. Lees‡ and Paul A. Flinn
Physics Department and Metals Research Laboratory, Carnegie-Mellon University, Pittsburgh, Pennsylvania 15213
(Received 11 September 1970)

The Mössbauer effect of Sn^{119} has been measured in alloys of the α-brass type: Cu-Sn, Cu-Sn-Zn, and Cu-Sn-Al. The isomer shift of the tin resonance is a function of the electron-to-atom ratio of the alloy, and is insensitive to the valence of the solute. The change in isomer shift with electron-to-atom ratio is rather small, but shows effects similar to those observed by soft-x-ray spectroscopy in α-brass, and by positron annihilation in α-copper-aluminum alloys.

I. INTRODUCTION

For many years, considerable effort has been expended to understand better the changes in the electronic densities of states upon alloying the noble metals with polyvalent metals. Conflicting experimental results, and disagreement between experiment and theory, have left the answer to the question still in doubt. The experimental work to date for the whole range of the α phase, rather than for only very dilute alloys, has been largely low-temperature specific-heat studies, and optical-absorption measurements,[1-7] with a limited amount of work using soft-x-ray spectroscopy[8] and positron annihilation.[9] Unfortunately, many of the

techniques available for studying pure metals are not available for alloy systems. Techniques such as the de Haas–van Alphen effect,[10] ultrasonic attenuation, cyclotron resonance, etc., require long electron mean free paths, which are only attainable in pure metals or very dilute alloys; techniques available for concentrated alloys are very limited in number.

In recent years, the Mössbauer effect has been shown to be a tool useful for studying the properties of solids, and in particular, the properties of metals. The purpose of this study is to provide additional information on noble-metal alloys by the use of the Mössbauer effect. The isomer shift of the Mössbauer resonance of a given nucleus is proportional to the change in the charge density at the nucleus, and, therefore, is dependent on the electronic environment. Thus, by studying the isomer shift of Sn^{119} in a number of alloys of copper, we were able to observe changes in the s character of the band wave functions, which are related to the electronic configuration of the tin atoms, and thereby detect changes in the band structure of the alloys with composition.

In order to relate the Mössbauer measurements, which give directly the charge density at the tin nuclei, to the changes in the band structure, we assume that the changes in the s character of the wave functions seen by the tin nuclei are essentially those of the Bloch waves. We feel that this is justified by the fact that the calculations of Soven[11] and of Amar, Johnson, and Sommers[12] for α-brass indicate that the conduction wave functions are well localized in momentum space.

II. DESCRIPTION OF ABSORBERS

In this study we used several series of copper alloys, all containing Sn^{119} as a probe. As solutes we used zinc, aluminum, and tin, which have valencies of 2, 3, and 4, respectively, in order to determine whether the changes observed depended primarily on electron-to-atom ratio, or on solute concentration.

The absorbers for the Mössbauer measurements were foils approximately 0.025 mm thick of Cu-Sn, Cu-Zn-Sn, and Cu-Al-Sn, prepared from 99.999% Cu, 99.999% Zn, 99.99% Sn, and 99.99% Al. Two different methods of sample preparation were used: induction melting, homogenization, and cold rolling to the desired thickness for the Cu-Sn and Cu-Al-Sn series, and a vapor transfer method for the Cu-Zn-Sn series.

The low boiling point of zinc (907 °C) makes it possible to introduce the zinc by vapor transfer and prepare alloys which all have essentially the same number of Sn^{119} atoms per cm^2. For each zinc composition, a master Cu-Zn alloy was prepared by induction melting and quenching. Brass chips from the master alloy were sealed in an evacuated Vycor tube along with a foil of Cu-Sn^{119} with dimensions roughly 25 mm square and 0.02 mm thick, and weighing 60–100 mg. The sealed capsule was placed in a furnace at the appropriate temperature, uniform within 5 °C over the length of the capsule, and maintained at temperature until the system was close to equilibrium. For alloys with compositions well away from the α-β phase boundary, two hours at 800 °C was sufficient for satisfactory transfer. Near the phase boundary, lower temperatures were used as required by the phase diagram. The zinc content was primarily determined by weighing the foil before and after the vapor transfer. At these temperatures, the vapor pressures of Cu and Sn are too low for any appreciable transfer to occur.

Two series of Cu-Zn-Sn alloys were prepared; one with a Cu–2%-Sn^{119} base foil, and the other with a Cu–$\frac{1}{2}$%-Sn^{119} base. The Cu-Sn-Al series of alloys contained 2% Sn^{119}. The binary Cu-Sn series were prepared entirely with enriched Sn^{119} for less than 2% total Sn, and with 2% Sn^{119} for the samples of higher tin content.

III. ANALYSIS OF SOLUTE CONCENTRATION

Since only nondestructive techniques could be used, lattice-parameter measurements and electron-microprobe analysis were used to check the compositions of the samples. The results are given in Table I. The microprobe results were corrected for background and dead time experimentally; the corrections for fluorescence, absorption, and atomic-number effects were based on the equations of Hammond, Davinson, and Jacobson.[13] For some samples, the high-concentration zinc, the high-concentration tin, and all the aluminum samples, the microprobe results are doubtful, owing to difficulties with surface roughness, wide disparities in atomic number, and slight oxide films on the aluminum-containing samples. These results are reported, but indicated as probably inaccurate, in the table.

As an additional check on the alloy compositions, the values of the lattice parameters as functions of the electron-to-atom ratio ($\mathfrak{z}$) based on nominal composition, are shown in Fig. 1. $\mathfrak{z}$ is calculated on the basis that each copper atom contributes one electron, each zinc two, each aluminum three, and each tin four. All four series of alloys lie on straight lines, with only two samples significantly off the lines. The $\mathfrak{z}$ values for these two samples, the Cu–5%-Sn and the Cu–1.5%-Sn, were corrected in accord with the lattice-parameter measurements. The corrected value for the 5% sample is also consistent with the microprobe result. The Cu-Sn line extrapolates correctly to the lattice parameter for pure copper, the Cu-Sn-Zn lines to the parameters for 2% Sn and $\frac{1}{2}$% Sn at 0% Zn, and the Cu-Al-Sn line to the parameter for 2.17% Sn, consistent with the

TABLE I. Sample compositions.

Alloy	Solute	Nominal composition			Composition (wt%)	
		at.%	wt%	$a_0(kx)$[a]	From lattice parameter	From microprobe
¼-Sn	Sn	0.27	0.51	3.6095	0.50 ± 0.05	•••
½-Sn	Sn	0.50	0.93	3.6111	0.93 ± 0.05	0.94 ± 0.05
1-Sn	Sn	1.02	1.90	3.6164	1.90 ± 0.05	•••
1.5-Sn	Sn	1.51	2.80	3.6194	2.52 ± 0.05	•••
2-Sn	Sn	2.01	3.70	3.6271	3.7 ± 0.1	3.6 ± 0.2
5-Sn	Sn	5.00	8.95	3.6525	8.2 ± 0.2	8.0 ± 0.2
9-Sn	Sn	8.67	15.05	3.6944	15.0 ± 0.2	13.0 ± 0.2[b]
10-XII	Zn	2.12	2.17	3.6154	2.2 ± 0.05	2.12 ± 0.1
	Sn	0.49	0.91			
7-1	Zn	4.74	4.85	3.6220	4.9 ± 0.1	•••
	Sn	0.48	0.89			
4-II	Zn	9.34	9.54	3.6304	9.4 ± 0.2	•••
	Sn	0.45	0.84			
24-I	Zn	2.47	2.49	3.6308	2.5 ± 0.1	3.0 ± 0.3
	Sn	1.96	3.61			
25-II	Zn	7.68	7.75	3.6407	7.8 ± 0.1	5.4 ± 0.4
	Sn	1.85	3.41			
26-XIII	Zn	9.34	9.43	3.6454	9.4 ± 0.1	9.3 ± 0.3
	Sn[x]	1.82	3.35			
23-IV	Zn	13.35	13.47	3.6526	13.4 ± 0.2	14.0 ± 0.4
	Sn[x]	1.75	3.21			
22-V	Zn	21.85	22.03	3.6719	22.5 ± 0.2	21.1 ± 0.3
	Sn[x]	1.57	2.89			2.6 ± 0.3
27-VIII	Zn	26.53	26.73	3.6800	26.5 ± 0.2	25.2 ± 0.4
	Sn[x]	1.48	2.71			2.3 ± 0.3
30-XVI	Zn	31.31	31.47	3.6903	31.5 ± 0.2	28.0 ± 1[b]
	Sn[x]	1.39	2.55			
32-XVII	Zn	41.75	41.90	•••	•••	35.0 ± 1[b]
	Sn[x]	1.15	2.11			
29-XIV	Zn	46.54	46.79	•••	•••	47.2 ± 1[b]
	Sn[x]	1.08	1.97			
5-Al	Al	5.01	2.15	3.639 ± 0.001	~5 at%	6.04
	Sn	2.00	3.78			3.26
10-Al	Al	10.04	4.44	3.648 ± 0.001	~10 at%	8.63
	Sn	2.01	3.91			3.47
15-Al	Al	14.99	6.83	3.6578	~15 at%	12.12
	Sn	2.00	4.01			3.62

[a]All values ± 0005kx unless otherwise specified ($1kx = 1.002\,06$ Å).
[b]Foil surface very uneven, microprobe results doubtful.

2.15% Sn content of the 5% Al alloy. In summary, the lattice-parameter measurements confirmed the nominal compositions for the Cu-Zn-Sn alloys, the Cu-Al-Sn alloys, and all but two of the Cu-Sn alloys. For these two alloys, the correct composition is taken to be that determined from the lattice-parameter measurement.

IV. EXPERIMENTAL RESULTS

The Mössbauer spectrometer and the iterative least-squares procedure (MFIT) for fitting the data were the same ones used for previous work and are discussed in detail elsewhere.[14] At least two peaks were used for each fit; in some cases, one or two additional small peaks were required to obtain a more satisfactory fit. The experimental data and the computer-calculated least-squares-fitted curves for several of the samples are shown in Fig. 2.

The isomer shifts for each of the two main peaks, their relative intensities, and the δ value for each sample are given in Table II. Except for two of the aluminum alloys, the values given are combined values obtained from several runs.

We assume that the presence of the secondary peak is a consequence of the presence of a variety of locally different tin environments. The effect of localization of charge about neighboring solute atoms can cause a change in the electronic structure at the tin site, and thus, a change in isomer shift. This peak actually represents an average value for many sites,

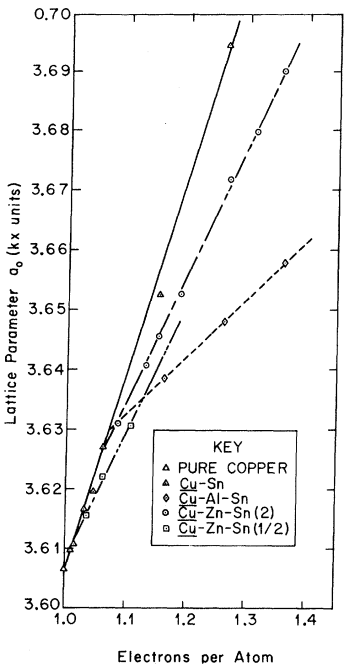

FIG. 1. Lattice parameter as a function of electron-to-atom ratio for the alloys studied ($1kx = 1.00206$ Å).

rather than indicating that there are only two different sites for the tin. We do not attempt a more detailed calculation for the distribution of the other solute atoms about the Sn probe, but merely note that the shifts of the secondary peak with composition follow those of the main peak.

Two sets of values for the positions of the main peaks in the Cu-Al-Sn spectra are reported in Table II. The first set of lines was obtained from the cold-rolled samples before annealing; the second set was obtained after annealing. There appear to be detectable cold-working effects in these alloys, especially at the higher concentrations, perhaps due to solute segregation at stacking faults. In the later discussion, the values obtained from the annealed samples are used. We were unable to detect any differences in the spectra from the Cu-Sn alloys before and after annealing. Since the method of preparation of the Cu-Sn-Zn alloys produced them already in the annealed condition, no such investigation was possible for that series.

A study of the changes in the main peak position, which is of primary interest, gives us some detailed information about the changes in electronic structure with composition occurring in copper alloys. The isomer shifts for the main peak for the various alloys are plotted as a function of ϑ in Fig. 3(a). It is evident that the isomer shift depends primarily on ϑ, rather than on solute concentration [cf. Fig. 3(b)]. Considered as functions of ϑ, the isomer shifts for nearby points agree within the standard deviations, with one exception, so that it is possible to accommodate all the points with a smooth band of reasonable width (cf. Fig. 4). In the case of Fig. 3(b), such a construction is not possible. The isomer shift shows an initial sharp rise from a value of -0.223 mm/sec at the lowest alloy concentration, to a relative maximum of -0.165 mm/sec at a ϑ value of about 1.06. This rise is followed almost immediately by a decrease to a flat minimum of -0.20 mm/sec beginning at a ϑ value of 1.12. At a ϑ value of about 1.2, the isomer shift again begins an increase to a value of about -0.145 near the α-phase boundary.

Using the calibration relation developed in earlier work,[14] we can estimate the change in s character, and the number of s-like tin valence electrons from these isomer shift values. We will assume that the tin atoms are approximately neutral with three p-like states localized around the tin. On this basis, the values for the number of s-like valence electrons corresponding to the maxima and minima of the isomer shift values are given in Table III.

Thus, over the whole range of the α phase, the tin nucleus sees a change of only 0.04 of an s-like electron, and there is always less than the equivalent of one $5s$ electron at the tin site. Other investigators[15–18] have also noted that the change of isomer shift of tin with composition within a single-phase alloy is quite small.

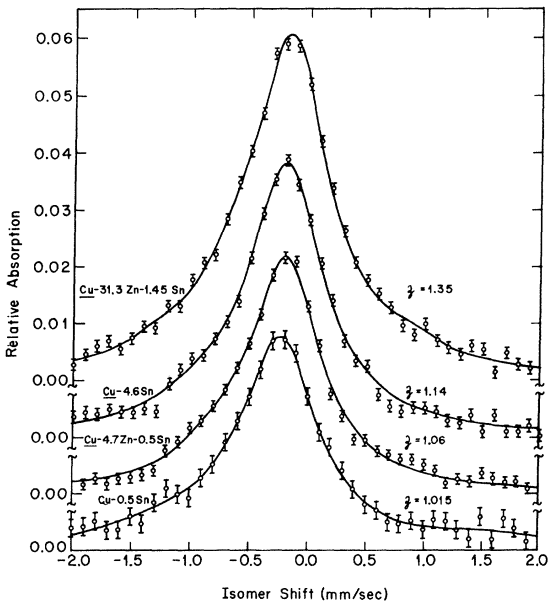

FIG. 2. Typical Mössbauer spectra for some of the alloys studied. Isomer shifts given relative to the Mg_2Sn source at 77 K, absorbers at room temperature.

TABLE II. Experimental results for the alloys. M is the main peak, S the secondary peak, B the peak before annealing, and A the peak after annealing.

Sample	ϑ	Peak	Isomer shift[a] (mm/sec)	Peak absorption (%)
$\frac{1}{4}$-Sn	1.008	M	−0.223 ± 0.013	3.03 ± 0.08
		S	−0.97 ± 0.11	0.41 ± 0.09
$\frac{1}{2}$-Sn	1.015	M	−0.214 ± 0.010	3.55 ± 0.10
		S	−0.88 ± 0.09	0.41 ± 0.09
1-Sn	1.031	M	−0.203 ± 0.007	9.40 ± 0.15
		S	−0.93 ± 0.05	1.23 ± 0.13
1.5-Sn	1.041	M	−0.196 ± 0.006	8.14 ± 0.18
		S	−0.80 ± 0.06	1.50 ± 0.17
2-Sn	1.060	M	−0.165 ± 0.007	6.75 ± 0.16
		S	−0.64 ± 0.06	0.89 ± 0.13
5-Sn	1.135	M	−0.196 ± 0.007	5.00 ± 0.08
		S	−0.90 ± 0.06	0.70 ± 0.08
9-Sn	1.260	M	−0.171 ± 0.008	9.95 ± 0.30
		S	−0.67 ± 0.06	1.72 ± 0.30
10-XII (Zn)	1.035	M	−0.199 ± 0.006	5.43 ± 0.07
		S	−0.85 ± 0.04	0.86 ± 0.07
7-I (Zn)	1.061	M	−0.186 ± 0.008	4.03 ± 0.08
		S	−0.77 ± 0.06	0.52 ± 0.08
4-II (Zn)	1.107	M	−0.172 ± 0.014	4.66 ± 0.30
		S	−0.57 ± 0.07	0.97 ± 0.30
24-I (Zn)	1.084	M	−0.175 ± 0.006	7.44 ± 0.12
		S	−0.78 ± 0.06	0.99 ± 0.12
25-II (Zn)	1.132	M	−0.196 ± 0.006	7.51 ± 0.09
		S	−0.83 ± 0.05	0.95 ± 0.10
26-XIII (Zn)	1.148	M	−0.188 ± 0.009	7.81 ± 0.16
		S	−0.79 ± 0.05	1.27 ± 0.16
23-IV (Zn)	1.186	M	−0.196 ± 0.005	8.79 ± 0.10
		S	−0.80 ± 0.03	1.41 ± 0.11
22-V (Zn)	1.266	M	−0.154 ± 0.011	6.21 ± 0.25
		S	−0.60 ± 0.08	0.97 ± 0.22
27-VIII (Zn)	1.310	M	−0.164 ± 0.011	6.42 ± 0.27
		S	−0.67 ± 0.08	1.26 ± 0.27
30-XVI (Zn)	1.355	M	−0.145 ± 0.010	5.56 ± 0.17
		S	−0.59 ± 0.05	1.12 ± 0.16
5-Al	1.160	M, B	−0.174 ± 0.008	8.61 ± 0.20
		S, B	−0.66 ± 0.05	1.35 ± 0.20
		M, A	−0.209 ± 0.019	9.3 ± 0.5
		S, A	−0.80 ± 0.06	1.3 ± 0.2
10-Al	1.261	B	−0.108 ± 0.014	6.2 ± 0.6
		B	−0.34 ± 0.05	3.3 ± 0.5
		B	−0.92 ± 0.09	0.74 ± 0.13
		M, A	−0.187 ± 0.008	10.2 ± 0.2
		S, A	−0.77 ± 0.05	1.45 ± 0.18
15-Al	1.360	B	−0.00 ± 0.04	4.3 ± 1.4
		B	−0.28 ± 0.08	4.8 ± 1.3
		B	−0.84 ± 0.07	1.4 ± 0.3
		M, A	−0.170 ± 0.018	8.0 ± 0.3
		S, A	−0.64 ± 0.03	3.2 ± 0.3
32-XVII	1.45(β)	M	−0.223 ± 0.009	4.70 ± 0.09
		S	−0.88 ± 0.06	0.62 ± 0.09
29-XIV	1.50(γ)	1	0.34 ± 0.04	1.52 ± 0.14
		2	−0.27 ± 0.02	4.44 ± 0.16
		3	−0.82 ± 0.07	0.72 ± 0.15

[a]Isomer shift relative to Mg_2Sn at 77 °K.

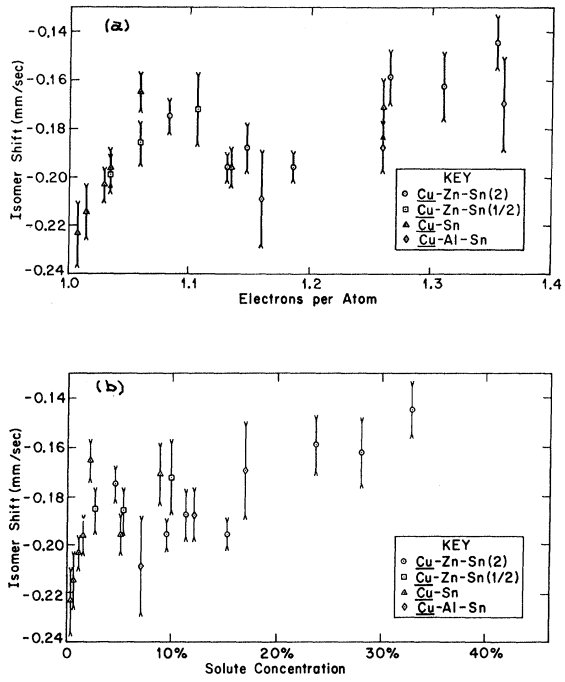

FIG. 3. Isomer shift as a function of electron-to-atom ratio for the alloys studied. The standard deviations shown are the results from the least-squares computer fittings. (b) Data of 3(a) replotted as a function of solute concentration.

V. DISCUSSION

Two other kinds of measurements on copper-base alloys show interesting similarities to the effects we have observed. A study of the x-ray absorption edges of copper-zinc alloys by Yeh and Azaroff[8] shows a decrease in the total densities of unpopulated s states with increasing ϑ. In addition, an anomaly (although not claimed as such by the authors) at the same place as ours appears in their data, as shown in Fig. 4. The total density of unpopulated s states decreases with increasing ϑ up to a ϑ value of about

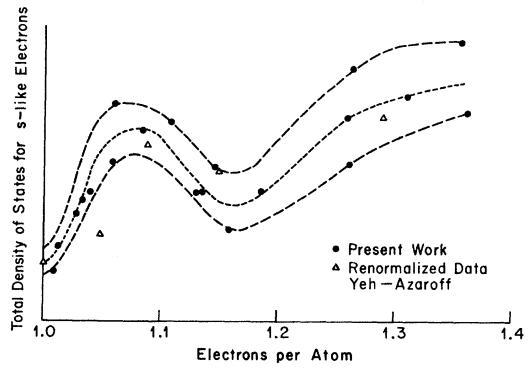

FIG. 4. Comparison of the Mössbauer results with the x-ray spectrographic data of Yeh and Azaroff (Ref. 8).

TABLE III. Extremal values of isomer shift and n_s.

Isomer shift	n_s
−0.223	0.93
−0.165	0.96
−0.200	0.94
−0.145	0.97

1.1; it then increases to a maximum in the ϑ range of 1.15–1.2, then decreases again to the phase boundary. Positron-annihilation measurements in Cu-Al alloys by Fujiwara, Sueoka, and Imura[9] show similar maxima and minima for certain dimensions of the Fermi surface. The neck radius, the ⟨111⟩ radius, and the ⟨100⟩ radius all show a rapid increase with a change of ϑ from 1.11 to 1.21; the neck radius also shows an initial rise from pure copper to a maximum at a ϑ value of 1.05.

Energy-band calculations for α-brass made independently by Soven[11] and by Amar, Johnson and Sommers[12] can be used to interpret the behavior we have observed experimentally. The two primary energy bands whose changes affect the density of states are the Γ_1 (primarily s-like) and L_2 (primarily p-like) bands. The level of the Γ_1 band decreases rapidly up to a ϑ of 1.1; it then continues to decrease, but at a slower rate, up to the phase boundary. The level of the L_2 band, on the other hand, decreases slowly up to a ϑ of 1.1; it then decreases much more rapidly up to a ϑ of 1.2. From this point to the phase boundary it again decreases more slowly, at about the same rate of decrease as that of the Γ_1 state.

From the behavior of these two bands, we would expect an initial sharp increase in the s-state density as the contact with the ⟨111⟩ zone boundary increases. This is also consistent with the increase in neck radius observed in the positron annihilation work. In the region from a ϑ of 1.1 to 1.2, the changes in the L_2 band dominate the density-of-states changes, and the states being filled are primarily p-like. From this we would expect at least a leveling off of the density of s-like states, and possibly a decrease in the s-like density, arising from hybridization effects, both in these bands, and also in the Λ_1 and Δ_1 bands. From a ϑ of 1.2 out to the phase boundary, we expect the s-like state density to increase again, but less rapidly than it did in the low-solute-content region.

The present data along with the soft-x-ray and positron-annihilation results can thus be qualitatively accounted for by the present theoretical models. It would be valuable, however, to have detailed information on the band wave functions, rather than merely energies, so that more detailed comparisons with experiments would be possible.

*Work supported in part by the U. S. Atomic Energy Commission.

†Work is based on a thesis submitted in partial fulfillment of the requirements for the degree of Doctor of Philosophy at the Carnegie Institute of Technology.

‡Present address: Plastics Department, E. I. du Pont de Nemours & Co., Parkersburg, W. Va. 26101.

[1]J. A. Rayne, Phys. Rev. 108, 22 (1957).
[2]J. A. Rayne, Phys. Rev. 110, 606 (1958).
[3]B. W. Veal and J. A. Rayne, Phys. Rev. 130, 2156 (1963).
[4]T. B. Massalski and L. L. Isaacs, Phys. Rev. 138, A139 (1965).
[5]M. A. Biondi and J. A. Rayne, Phys. Rev. 115, 1522 (1959).
[6]B. A. Green, Phys. Rev. 144, 528 (1966).
[7]L. C. Clune and B. A. Green, Phys. Rev. 144, 525 (1966).
[8]H. C. Yeh and L. V. Azaroff, J. Appl. Phys. 38, 4034 (1967).
[9]K. Fujiwara, O. Sueoka, and T. Imura, J. Phys. Soc. Japan 24, 467 (1968).
[10]P. E. King-Smith, Phil. Mag. 12, 1123 (1965).
[11]P. Soven, Phys. Rev. 151, 539 (1966).
[12]H. Amar, K. H. Johnson, and C. B. Sommers, Phys. Rev. 153, 655 (1967).
[13]M. L. Hammond, A. T. Davinroy, and M. I. Jacobson, Technical Report No. AFML-TR-65-223, 1965 (unpublished), p. 69.
[14]J. K. Lees and P. A. Flinn, J. Chem. Phys. 48, 882 (1968).
[15]S. L. Ruby, H. Montgomery, and C. W. Kimball, Phys. Rev. B 1, 2948 (1970).
[16]B. I. Verken, V. V. Chekin, and A. P. Vinnekov, Zh. Eksperim. i Teor. Fiz. 51, 25 (1966) [Soviet Phys. JETP 24, 16 (1967)].
[17]B. Window, J. Phys. C 2, 1 (1969).
[18]M. Cordey Hayes and I. R. Harris, Phys. Letters 24A, 80 (1967).

PHYSICAL REVIEW B VOLUME 3, NUMBER 3 1 FEBRUARY 1971

Three-Dimensional Scattering Analysis of Field Emission from a Tip. I. The Unperturbed Model*

Jay L. Politzer
Computation Center, The Pennsylvania State University, University Park, Pennsylvania 16802

and

T. E. Feuchtwang
Department of Physics, The Pennsylvania State University, University Park, Pennsylvania 16802

(Received 13 March 1970)

A formulation of field emission from a spherical tip is developed in terms of scattering theory. It is shown that in three dimensions the usual "transmission coefficient" is replaced by a differential scattering probability. The statistical average over the Fermi distribution is obtained without recourse to the usual kinetic arguments, which are shown to lack general validity. The zero-order problem is taken to be emission from a spherical well through a Coulomb barrier. This problem is solved exactly. The energy distribution of the field-emitted electrons is calculated for this model and found to be always larger than that calculated for the one-dimensional triangular barrier. In a second publication, more realistic models are analyzed in terms of a distorted-wave Born approximation which utilizes the solutions of the present problem.

I. INTRODUCTION

Recent work in field emission has stressed the observation and understanding of band-structure effects in the energy distributions of emitted electrons. This work is motivated by a desire to relate the observed distributions to the band structure of the emitting crystal. One impediment to an understanding of band-structure effects is that the only relevant experiment is field emission from fine needles or tips, while all of the theory has been developed for field emission from planar surfaces. Nevertheless, present indications from both theory and experiment are that band-structure effects do play a part in field emission, and that these effects are observable. Quantitative comparisons between theory and experiment are difficult to justify owing to the planar geometry used in the theory. In this paper, a three-dimensional theory of field emission is developed to account for more realistic emitter shapes. However, no attempt is made to account for the band structure of the emitter. We can assert, therefore, that differences between the present three-dimensional theory and experiment are probably due to band-structure effects alone, and are less likely to be attributable to the näive geometry of the theory. Conversely, it is not valid to assume that anomalies in field-emission data are due to band-struc-